# Comparison of aluminium foams prepared by different methods using X-ray tomography

Ningzhen Wang, Éric Maire, Ying Cheng, Yasin Amani, Yanxiang Li, Jérôme Adrien, Xiang Chen

# Comparison of aluminium foams prepared by different methods using X-ray tomography

Ningzhen Wang[a], Eric Maire[b], Ying Cheng[a], Yasin Amani[b], Yanxiang Li[a,c], Jérôme Adrien[b], Xiang Chen[a,c,*]

[a] *Department of Materials Engineering, School of Materials Science and Engineering, Tsinghua University, Beijing 100084, China*
[b] *INSA de Lyon, MATEIS CNRS UMR5510, Université de Lyon, 69621 Villeurbanne, France*
[c] *Key Laboratory for Advanced Materials Processing Technology (MOE), Tsinghua University, Beijing 100084, China*

The cell structure and mechanical properties of aluminium foams prepared by melt foaming (MF) method are supposed to be better than the ones produced by gas injection (GI) method. Preparation processes of these two methods have been developed during the last recent years. Mechanical properties of aluminium foams depend strongly on characteristics of the cell structure. Therefore, it is necessary to compare cell structures of the foams fabricated with these two methods quantitatively using X-ray computed tomography and this is the purpose of the present paper. MF and GI foams have thus been prepared. True density measurements and cell structures indicate that the volume fraction of the closed cells of MF foam with high porosity is negligible. By contrast, the majority of cells of GI foam are closed. Results of cell structure analysis show that there are more micropores in cell walls of the foams prepared by MF method compared to the ones prepared by GI method, especially for the MF foams with low porosity. In addition, results of cell size study show that the cell size distribution is wide in dynamic GI foams, and there are usually big holes inside MF foams. GI method is more suitable to prepare aluminium foams with high porosity compared to MF method. Furthermore, the thickness difference between normal cell wall and Plateau border is greater in GI foams, in particular for the ones produced by the static injector.

## 1. Introduction

Melt foaming (MF) and gas injection (GI) are two important methods to prepare aluminium foams [1,2]. In the MF procedures, a blowing agent (e.g. $TiH_2$) is added into the thickened molten aluminium and the aluminium foam is obtained by decomposition of the blowing agent and subsequent solidification of the molten aluminium (this is the method used to produce the ALPORAS foams [3]). In the GI method, a gas jet is driven directly into the molten aluminium using a nozzle, and ceramic particles are contained in the molten aluminium for bubbles stability. There are two versions of this process, namely the dynamic and the static versions depending on the fact that the GI needle is moving or static. The first dynamic GI methods were developed by Alcan [4,5] and Norsk Hydro [6], and the static method by HKR [7,8]. The cells of aluminium foams prepared by these two ways are usually considered to be closed because they are originated from isolated gas bubbles [9]. Closed-cell aluminium foams have wide application prospects in aerospace, automobile and building industries due to their properties, e.g. low density, good energy absorption performance, effective noise reduction and fire resistance [10]. The MF is a simpler preparation process, especially for producing large foam blocks, so it is more popular in industry. GI is relatively low cost and has the advantage of continuous production [11]. Other researchers have compared aluminium foams prepared by different ways. Y. Sugimura et al. [9] found that the cell size and cell wall thickness of the Alporas foam were both smaller compared to the Alcan foam with a similar porosity. A.E. SIMONE et al. [12] concluded that Alporas foams had a better cell structure and mechanical properties compared to Alcan foams. A. Elmoutaouakkil et al. [13] characterised various aluminium foams using X-ray tomography and found that cells of Alporas foams and Norsk-Hydro foams were both closed, and Norsk-Hydro foams presented a bimodal cell size distribution. Most of the previous studies showed that MF foams are usually superior to GI foams concerning the homogeneity of both their structure and properties [1,9,12,13].

If the mechanical properties of aluminium foams could be improved, certainly their applications can be further expanded [3,10,14].

* Corresponding author.
*E-mail address:* xchen@tsinghua.edu.cn (X. Chen).

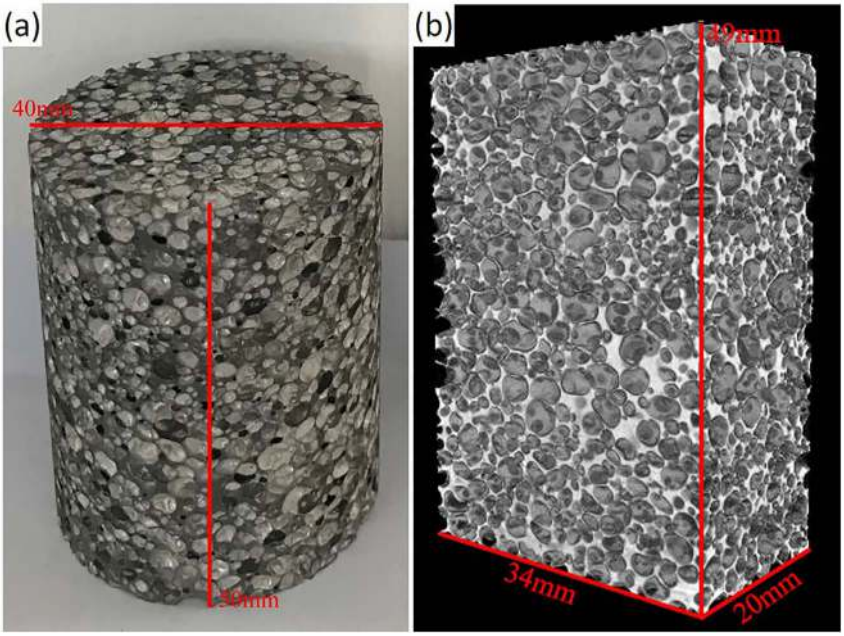


**Fig. 1.** (a) The macrographic photograph of a GI foam (sample No. 9 in Table 1), (b) 3D view of the corresponded sample after cropping.

Mechanical properties of aluminium foams could be improved from the matrix alloy [15] or cell structure, which includes relative density, cell morphology and cell size, and their influences are usually not independent of each other [16,17]. In recent years, reducing the cell size of aluminium foams is an effective and extensive way to improve mechanical properties, both in MF [18,19] and dynamic GI [20–24] methods. With the developments of aluminium foam preparation technology and characterising technique in the last few years, it is necessary to systematically inspect the cell structure differences of aluminium foams prepared by different methods, especially when the average cell diameter is decreased to around 1 mm [19,23]. If this is achieved, the effect of cell structures could be quantitatively analysed in the mechanical property study of different aluminium foams [25], then the application of aluminium foams prepared by different ways could be better carried out according to their different cell characteristics.

X-ray computed tomography (XRCT) is a nondestructive and effective way to characterise the cell structure of aluminium foams [26–29]. The acquisition of 3D images helps to analyse the morphology of the foams quantitatively and accurately. Gas trapped in the closed cells influences the compressive performance [30], especially in the dynamic response [31]. So it is necessary to try to detect the micro connections between the cells and measure the amount of closed and open porosity accurately, which is beneficial to the prediction and study of mechanical properties of different aluminium foams. Micropores in cell walls and Plateau borders would affect the failure process of aluminium foams under compressive loads [32]. Moreover, M. Mukherjee et al. [33] defined microporosity and pointed out that micropores promote the generation of macro defects, such as broken cell walls. The cell size distribution is also an important parameter [8,13], which can affect the energy absorption ability of aluminium foams [34]. The sphericity of pores affects the effective conductivity (both thermal and electrical) and Young's modulus of closed cell metallic foams [35]. Distribution of the cell wall thickness depends on the preparation of aluminium foams; it certainly influences the deformation and failure of cells [36–38]. Therefore, the above parameters are worth studying in the comparison of aluminium foams prepared by different methods.

In this paper, aluminium foams prepared by MF method [19], static GI [39] and new dynamic GI methods [23] are studied by X-ray tomography. Closed porosity, micropores distribution, cell size and solid material thickness distributions of these foams are compared quantitatively. The comparison of aluminium foams prepared by different ways is significant for optimizing the mechanical property and extending the future application of aluminium foams.

## 2. Experimental

Fourteen aluminium foam specimens, which were all prepared by the authors, were used for X-ray tomography experiments in this paper. In the case of the MF method, five samples with different cell sizes were selected, and the cell size was reduced by mixing the pre-oxidized $TiH_2$ with Cu powder. A more detailed description is given in literature [19]. In the case of the static GI method, three samples with different cell sizes were chosen. A foam sample with the minimum cell diameter (around 5 mm) was obtained by the optimization of orifice diameter and chamber pressure during the static GI process, as described in detail in literature [39]. In the case of the dynamic GI method, six samples with different cell sizes were chosen. A self-developed high-speed horizontal oscillation system was used in the preparation procedure [40], and a specimen prepared by the combination of high-speed horizontal oscillation and improved melt preparation methods (smaller particle size and less particle addition) was also scanned [23]. In order to improve the scanning resolution and facilitate the analysis of cell wall structure, samples were cut to certain sizes. For the reliability of average cell parameters, the dimensions of the scanning samples were determined by ensuring a sufficient number of cells (at least ten cells) in each direction. The foam samples are all cylindrical, as shown in Fig. 1(a). They were weighed by an electronic balance. Then, the porosity of the foam could be obtained by Eq. (1).

$$P = 1 - \frac{4m}{\pi d^2 \cdot h \cdot \rho_s} \tag{1}$$

where $P$ is the measured porosity according to the relative density of the aluminium foam specimen, $m$ the weight, $\rho_s$ the solid density, $d$ and $h$ the diameter and height of the cylindrical foam sample, respectively. For simplicity in this paper, the solid densities were taken as the expected densities of the aluminium alloy matrices (pure aluminium 2.7 g/cm$^3$ and A356 aluminium alloy 2.685 g/cm$^3$ for MF and GI foams, respectively). We are aware however of the fact that this density also actually slightly depends on the additives, but we will neglect this small

**Table 1**
Preparation methods and physical parameters of the foam samples for X-ray tomography.

| Number | Diameter (mm) | Height (mm) | Measured porosity (%) | Preparation method | Matrix |
|---|---|---|---|---|---|
| 1 | 40 | 50 | 76.7 | MF method | Pure aluminium |
| 2 | 50 | 62.5 | 81.1 | MF method | Pure aluminium |
| 3 | 50 | 62.5 | 84.4 | MF method | Pure aluminium |
| 4 | 30 | 37.5 | 54.8 | MF method | Pure aluminium |
| 5 | 40 | 47.5 | 76.8 | MF method | Pure aluminium |
| 6 | 50 | 62.5 | 85.9 | Static GI method | A356 alloy |
| 7 | 80 | 100 | 88.9 | Static GI method | A356 alloy |
| 8 | 80 | 100 | 95.5 | Static GI method | A356 alloy |
| 9 | 40 | 50 | 75.9 | Dynamic GI method | A356 alloy |
| 10 | 50 | 58 | 81.0 | Dynamic GI method | A356 alloy |
| 11 | 50 | 62.5 | 85.3 | Dynamic GI method | A356 alloy |
| 12 | 60 | 55 | 84.3 | Dynamic GI method | A356 alloy |
| 13 | 50 | 62.5 | 91.9 | Dynamic GI method | A356 alloy |
| 14 | 50 | 62.5 | 85.6 | Dynamic GI method + smaller particles (3.7 μm) | A356 alloy |

effect. Preparation methods and physical parameters of the specimens used for X-ray tomography scanning are listed in Table 1.

The laboratory X-ray tomography equipment used in this work is located in the MATEIS lab of INSA Lyon and manufactured by Phoenix X-ray company. The voltage was set to 80 kV, and the intensity 280 μA during all the scanning procedures. The detailed description of the tomography equipment was given in [41,42]. The resolutions of the scanning were chosen to be 30–77 μm per voxel depending on the overall sizes of the samples. Moreover, for further investigation of the structure of cell walls, some selected foams were also scanned at higher resolutions (4–6.3 μm per voxel for different foams), in the so called "local" tomography mode. We have verified that in the case of our studied foams, local tomography is not detrimental to resolution. The 3D images of the foams could then be obtained after reconstruction via the commercial software coupled to the tomography equipment.

Subsequent processing of the 3D images was performed via Fiji software according to the following procedures:

- First, the parallelepipedic 3D region containing only foam and no outside air was cropped from the cylindrical shape of the sample, as shown in Fig. 1(b). From this representative volume, cells were binarized using a simple threshold. All the following calculations were performed on the binarized image.
- Then, porosity was calculated by dividing the amount of white voxels (corresponding to the cells) over the total number of voxels of the analysed volume.
- After that the pores were labeled using a home-made plugin (called "Labelling 3D") to identify the completely closed cells, including micropores.
- In order to retrieve the typical size distribution of the possibly connected cells, the Fiji plugin "Local Thickness" was used [43,44]. This mathematical morphology measurement, also sometimes called "granulometry" procedure, allows us to retrieve the thickness distribution of connected 3D objects with complex shapes.
- At this stage, "Local Thickness" plugin on the solid (completely connected) phase was also used to measure the solid material thickness distribution of the aluminium foams.
- Finally, the connected cells were virtually splitted using the Fiji plugin called "3D watershed split" [45]. The morphological parameters (volume, surface, sphericity, inertia moments, orientation etc.) of each splitted cell were then calculated using a second home-made plugin (called "Param 3D").

To experimentally measure the difference of overall closed porosities of MF and GI foams, a true density experiment was performed. A JW-M100A true density meter implementing the gas expansion replacement method was used, wherein the used gas was He. The volume of open pores could be estimated by measuring the volume of the replaced gas, which lead to calculating the closed porosity.

## 3. Results and Discussion

### 3.1. Porosity Obtained by Tomography Result

In order to verify the reliability of the binarization results, the porosity obtained by tomography was compared with the porosity obtained by relative density of the foam sample in Table 1, as shown in Fig. 2.

It is clearly shown that the porosity from tomography agrees well with the porosity from relative density. Therefore, the tomography result and binarized 3D image successfully describe the structure of the aluminium foams. Taking into account the errors in the values of solid densities and measurement of foam dimensions for the porosity obtained by relative density, the porosity values obtained by tomography result were used in the rest of the paper, which were believed more reliably trusted. The two porosity values of different aluminium foam samples are listed in Table 2 to facilitate comparison, and the numbers of the samples are consistent with that in Table 1. In order to better distinguish different samples, each foam sample is named according to their preparation method and porosity, as shown in Table 2.

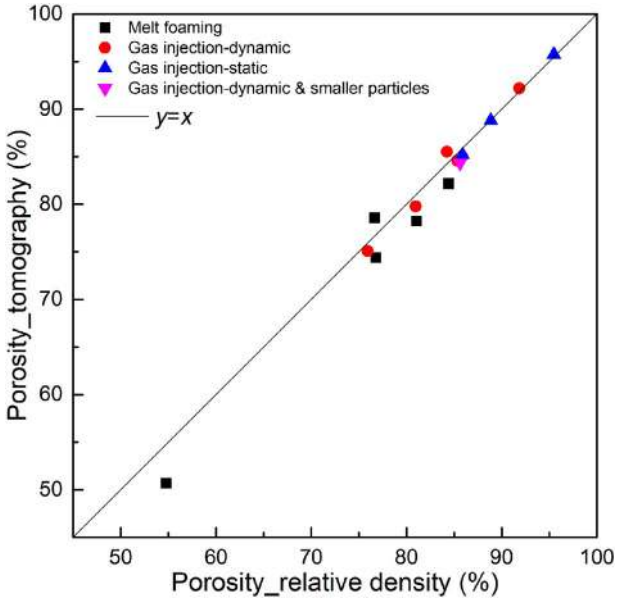


**Fig. 2.** Comparison of porosities obtained by tomography images and relative densities.

**Table 2**
The two porosity values of different aluminium foam samples.

| Number | 1 | 2 | 3 | 4 | 5 | 6 | 7 |
|---|---|---|---|---|---|---|---|
| Porosity_relative density (%) | 76.7 | 81.1 | 84.4 | 54.8 | 76.8 | 85.9 | 88.9 |
| Porosity_tomography (%) | 78.6 | 78.2 | 82.2 | 50.7 | 74.4 | 85.2 | 88.8 |
| Name | MF79 | MF78 | MF82 | MF51 | MF74 | GI85sta | GI89sta |
| Number | 8 | 9 | 10 | 11 | 12 | 13 | 14 |
| Porosity_relative density (%) | 95.5 | 75.9 | 81.0 | 85.3 | 84.3 | 91.9 | 85.6 |
| Porosity_tomography (%) | 95.8 | 75.1 | 79.8 | 84.6 | 85.5 | 92.2 | 84.4 |
| Name | GI96sta | GI75dyn | GI80dyn | GI85dyn | GI86dyn | GI92dyn | GI84dyn |


**Fig. 3.** The two aluminium foam specimens for true density experiments.

### *3.2. Closed Porosity Difference of Aluminium Foams Prepared by Different Methods*

Two aluminium foam samples prepared by MF and GI methods were tested by the true density meter, the specimens are shown in Fig. 3. Diameter of the two samples is 40 mm, and their height is 50 mm. Open porosity can be calculated by the replaced gas in the true density experiment, then the closed porosity can be obtained combined with the overall porosity of the foam. Physical parameters and true density test results of the two foams are listed in Table 3. It is shown that almost all cells of the aluminium foam prepared by MF method with the current porosity are open. On the other hand, except from the open cells on the outer surface, the cells inside the aluminium foam prepared by GI method are mostly closed. The closed porosity difference of aluminium foams prepared by different methods can be further described by the morphology of cell walls.

In order to describe this morphology, foam samples prepared by different methods were scanned at higher resolutions of 4–6.3 μm per voxel, as shown in Fig. 4. Fig. 4(a) and (b) show that there are many small gaps in cell walls of MF foams, which were marked by circles, and these gaps lead to the interconnections of cells. In the case of GI foams, gaps in cell walls hardly appear even though the cell walls are very thin, namely almost all cells are complete in the 2D view, as shown in Fig. 4(d), (e) and (f). Fig. 4 shows only one slice of every scanning sample. If the slices with some small gaps in cell walls stack into a 3D view, it means that many cells are connected together in the 3D view, which could be described by the structure in Fig. 5(a). The cells connected with each other through small holes in cell walls, as marked by A, B, C, D and E in Fig. 5(a). Fig. 5(b) describes a representative individual cell. A large number of interconnected cells in MF foams reduce the closed porosity. On the contrary, many individual cells guarantee the closed porosity of GI foams. Moreover, the entrapped gas inside closed-cells contributes to the compressive performance of aluminium foams [30,31], so the interconnected cells which reduce the amount of this entrapped gas are likely to be detrimental to the mechanical properties. When the porosity of the MF foam is low, and cell walls are thick, the cell connections through cell walls decrease, as shown in Fig. 4(c) (the resolution is 4 μm per voxel). For foam samples studied in this paper, most internal cells of all the GI foams are closed, and only MF51 has a high closed porosity for MF foams.

**Table 3**
Physical parameters and true density measurement results of the two aluminium foams prepared by different methods.

| Samples | Total porosity (%) | Open porosity (%) | Closed porosity (%) |
|---|---|---|---|
| A: MF | 76.7 | 74.49 | 2.21 |
| B: GI | 86.1 | 28.04 | 58.06 |

It is quite straightforward to infer that the gaps in cell walls of MF foams are mainly formed during the solidification shrinkage process of cells. In the case of GI foams with nearly no gap in cell walls it is possible that the gas forming bubbles is actually a quite oxidizing gas (usually it is air). As a consequence of this oxidisation nature, the surface of bubble wall could be covered by a layer of oxide film [46,47]. Then the oxide film with toughness would prevent the tearing of bubble walls in the process of solidification shrinkage, even though the thinning of bubble walls appears. In the case of the MF method, the gas

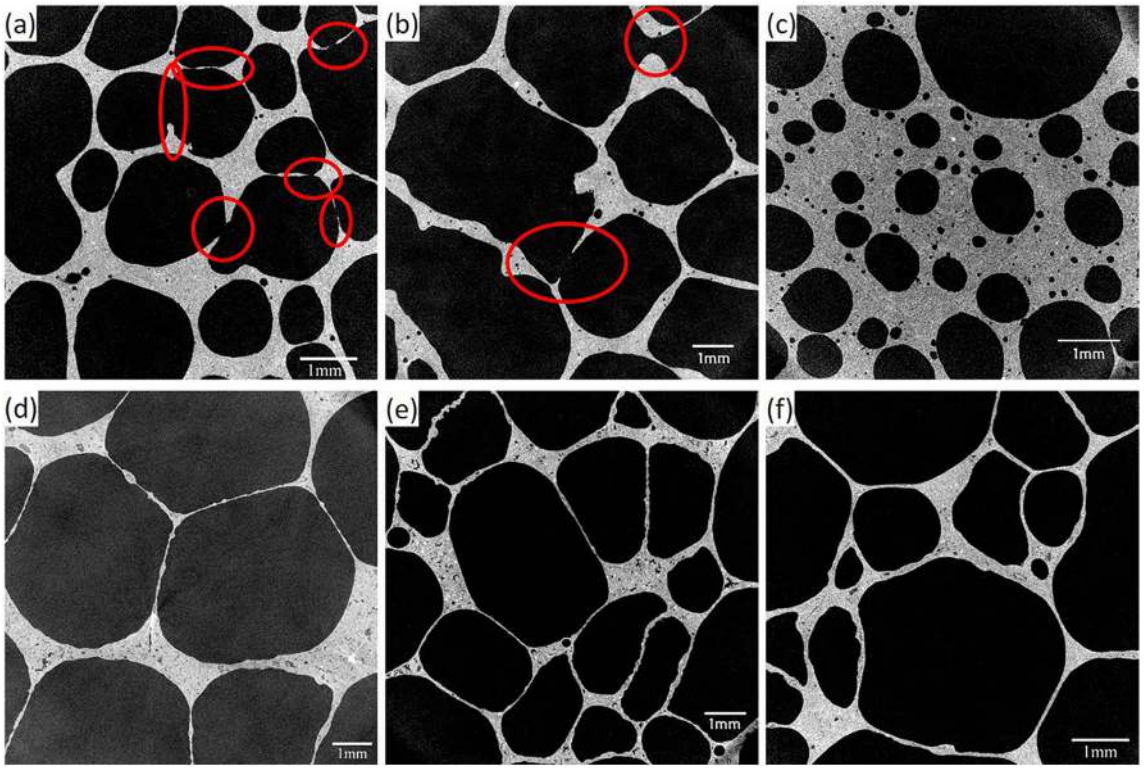


**Fig. 4.** High resolution XRCT slices showing the cell wall morphology of (a) MF79, (b) MF 78, (c) MF51, (d) GI85sta, (e) GI80dyn and (f) GI75dyn.

forming the bubbles is hydrogen. In the process of solidification shrinkage, the bubble wall is easily torn after thinning without the protection of oxide film. And the small gaps (in 2D image) or small holes (in 3D image) will appear in the cell wall after solidification, then the cells will be connected by small holes in cell walls. When the relative density of MF foams is high, the bubble wall is thick enough and not easy to be torn during the solidification process. So the connection of cells can be reduced when the overall porosity is low enough. Consequently, GI method allows the cells of aluminium foams to be completely closed at a higher porosity compared to MF method.

### *3.3. Comparison of Micropores in Aluminium Foams Prepared by Different Methods*

Fig. 4 shows that there are some micropores in cell walls and Plateau borders, which would affect the mechanical properties of aluminium foams. So it is necessary to study the distribution and amount of micropores in different aluminium foams. The completely closed pores in the binarized image could be distinguished by "Labelling 3D" plugin, as shown in Fig. 6, then the morphological parameters of every closed cell could be obtained by "Param 3D" plugin. The threshold setting during binarization process has a certain degree of subjectivity, so thin cell walls between large cells are hard to be recognised by the software. Because most of the micropores are closed with thick walls, the micropores in aluminium foams could be distinguished by this plugin easily. It has been studied that micropores with 30 μm to 350 μm in diameter are crack originations [32]. Based on this research result, M. Mukherjee et al. [33] defined the equivalent diameter of micropores as $\leq 350$ μm, and the same definition for micropores was used in this paper. Therefore, the information of micropores could be extracted from the morphological parameters results. It can be concluded from Fig. 6 that the volume fraction of micropores in

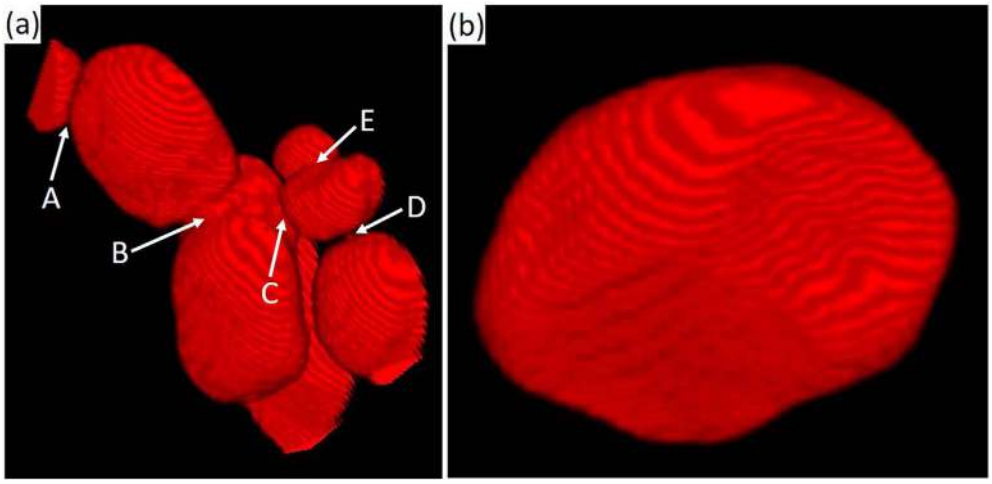


**Fig. 5.** (a) A structure of interconnected cells, (b) a representative individual cell.

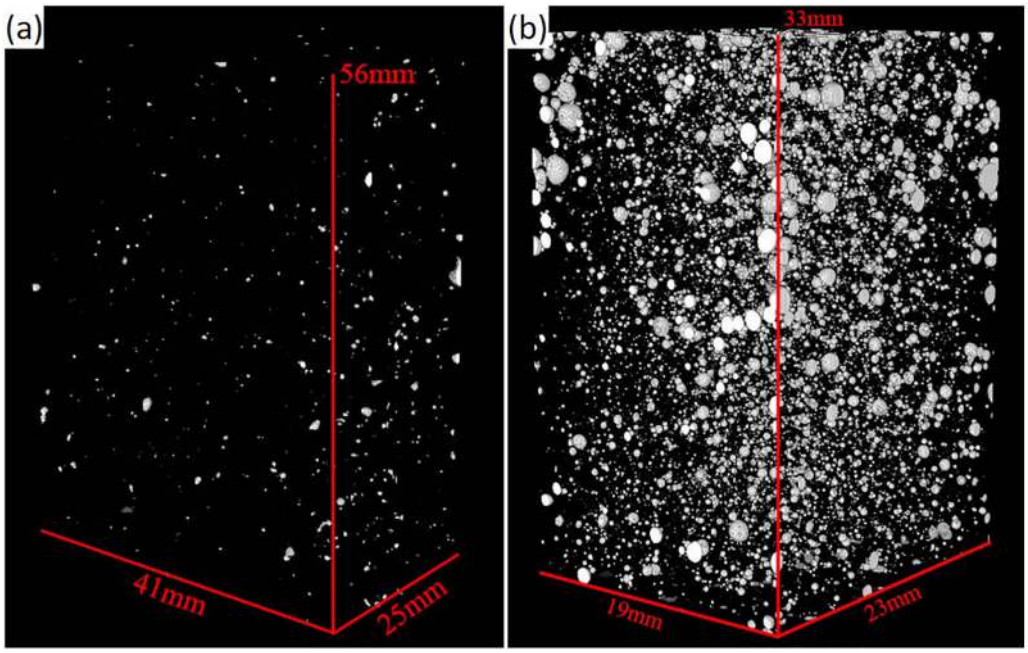


**Fig. 6.** 3D images of (a) GI80dyn and (b) MF51 after labelling.

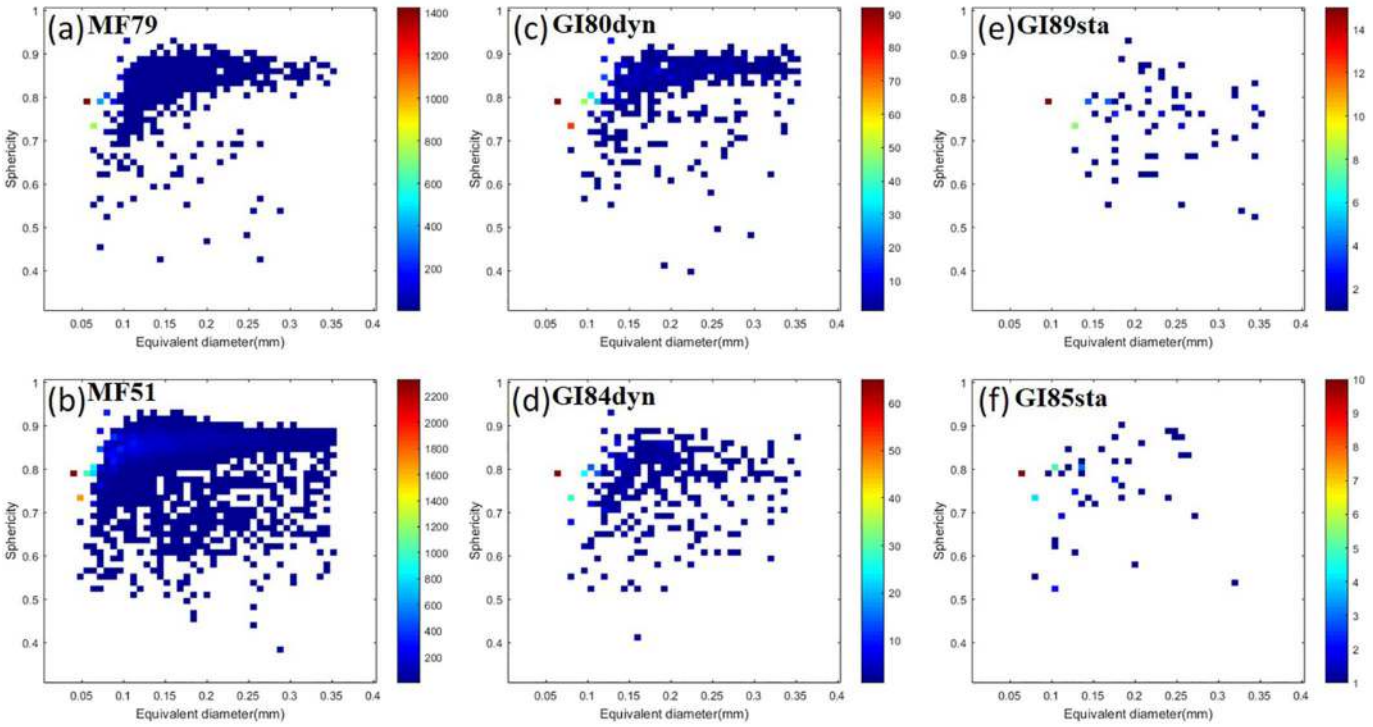


**Fig. 7.** Distributions of equivalent diameter and sphericity of micropores in different aluminium foams, (a) MF79, (b) MF51, (c) GI80dyn, (d) GI84dyn, (e) GI89sta and (f) GI85sta.

the MF foam is much higher than that in the GI foam.

Fig. 7 shows the equivalent spherical diameter as a function of the sphericity of each micropore in six different foam samples (chosen as being representative of the 14 foam samples). It is clearly shown in Fig. 7 that micropores in MF foams are much more numerous than the ones in GI foams, especially when the overall porosity is low, as shown in Fig. 7(b). Number of micropores in static GI foams is less than the one in dynamic GI foams. The sphericities of most micropores in different aluminium foams are concentrated in 0.7–0.9 (for a perfect sphere the value is 1). The good sphericity of the micropores indicates that the proportion of micropores caused by solidification shrinkage is small. Regardless of the micropores formed in the shrinkage process, difference of the number of micropores can be explained by the preparation processes of different foams.

In the case of the MF method, it was difficult to perfectly uniformly disperse $TiH_2$ probably because of the poor wettability between $TiH_2$ and aluminium melt. The contact angle between $TiH_2$ and aluminium melt is about 153° [48]. The particle size of $TiH_2$ powder used in our preparation is < 48 μm [19]. Therefore, it is difficult to disperse $TiH_2$ evenly in the preparation process, and although we have no real proof of this assertion, there will likely be both aggregated and dispersed blowing agents in the melt. The aggregated blowing agent formed

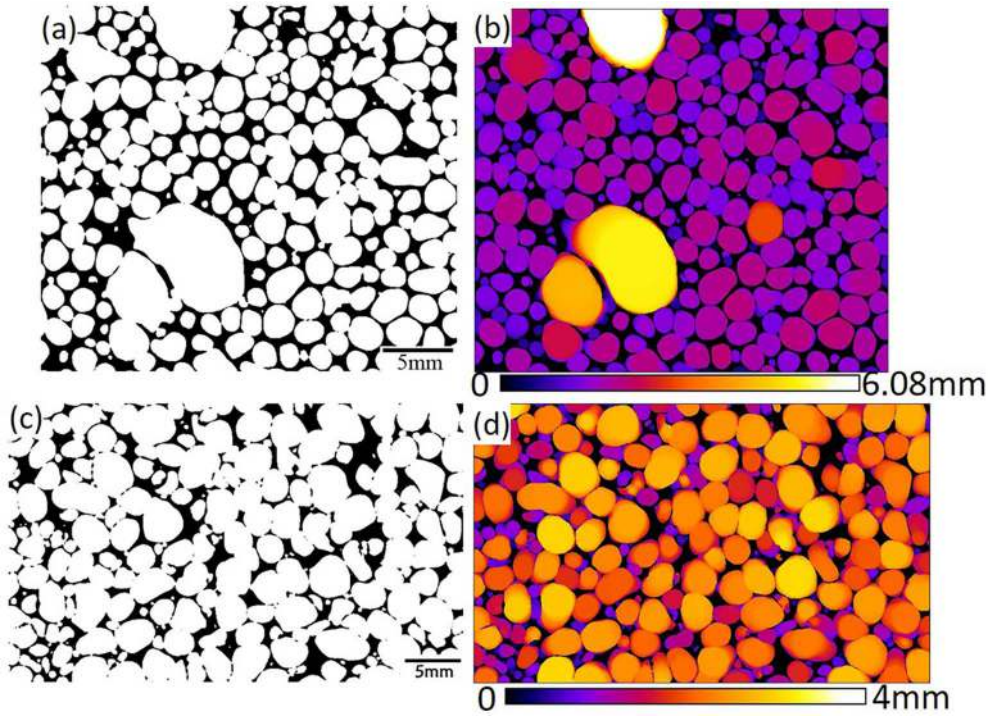


**Fig. 8.** (a) Binarized image and (b) the image after calculating with "Local Thickness" of the MF74 (the calculated average cell size $\bar{d}$ with this method is 1.73 mm, and the standard deviation $s$ is 0.606 mm), (c) binarized image and (d) the image after calculating with "Local Thickness" of the GI80dyn ($\bar{d}$ is 2.08 mm, and $s$ is 0.619 mm).

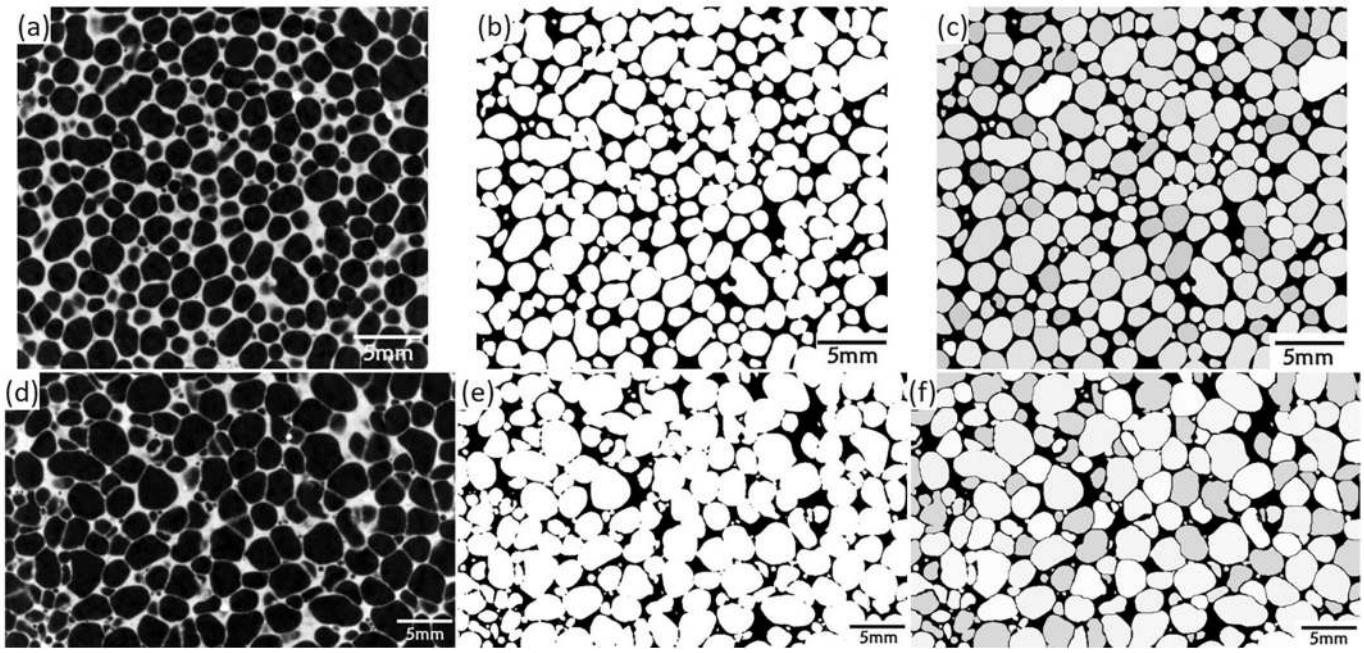


**Fig. 9.** Cell split processes of (a)–(c) the MF74 (the calculated average cell size with this method is 1.89 mm, and the standard deviation $s$ is 0.462 mm) and (d)–(f) the GI80dyn ($\bar{d}$ is 2.62 mm, and $s$ is 0.696 mm). (a) and (d) are original scanned 2D images, (b) and (e) are images after binarization, (c) and (f) are images after using "3D watershed split".

larger bubbles, the dispersed blowing agent formed micropores. The micropores which did not merge with large pores during the drainage process would remain on the cell walls. In the preparation of the aluminium foam with lower porosity, less amount of blowing agent resulted in more dispersed $TiH_2$ in the molten aluminium. So there are more micropores in the aluminium foam with low porosity. In the case of the GI method, the large cells were formed by the bubbles generated from the gas injection needle, and micropores in cell walls were mostly formed by the air present in the molten aluminium alloy or rolled from molten surface. The high-speed horizontal oscillation needle of dynamic GI method causes the disturbance of molten aluminium alloy inevitably, and more air will be involved in the foaming melt. So the fraction and density of micropores in dynamic GI foams are higher than that in static GI foams. Obviously, micropores formed by the air in melt in GI foams are less than the ones formed by the decomposition of $TiH_2$ in MF foams.

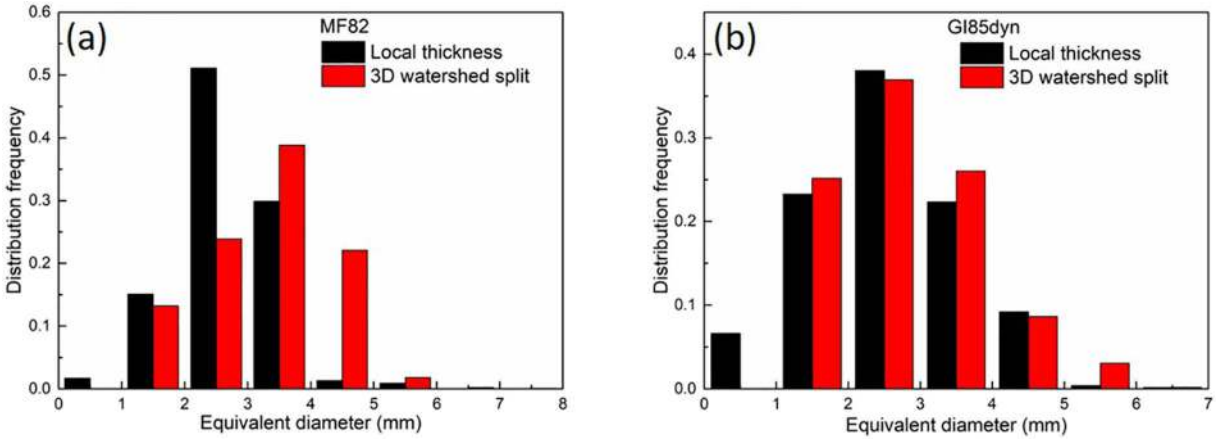


**Fig. 10.** Distribution comparisons of the cell equivalent diameters obtained by "Local Thickness" and after "3D watershed split" for (a) MF82 and (b) GI85dyn.

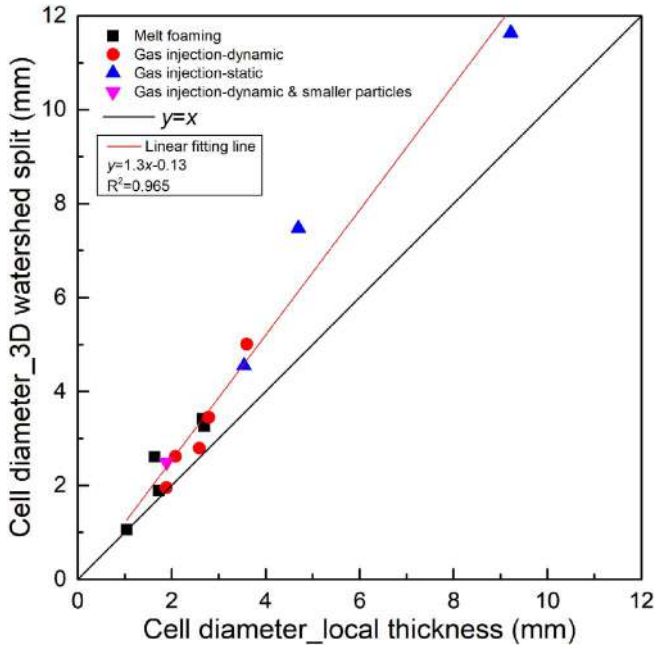


**Fig. 11.** Comparison of the average cell equivalent diameters obtained by "Local Thickness" and after "3D watershed split".

### *3.4. Cell Size Difference of Aluminium Foams Prepared by Different Methods*

As mentioned above, there are some connections between the cells in aluminium foams, in particular for the MF foams, as shown in Fig. 4(a) and (b). "Local Thickness" plugin can be used to obtain the size distribution even if the cells are connected. Fig. 8 shows typical results after such measurements of "Local Thickness". The colour in the graph is equal to the thickness measured. It is clear here that even if the cells are connected, their typical diameters can be measured by this method. Another method was to split the connected cells using the plugin of "3D watershed split" first, as shown in Fig. 9. Then the plugin of "Param 3D" could be used to obtain the equivalent diameter and sphericity of every independent cell.

Fig. 10 shows the distribution comparisons of the cell equivalent diameters obtained by "Local Thickness" and "Param 3D" after "3D watershed split" for samples MF82 and GI85dyn. The cell size distributions obtained by the two methods in the sample of Fig. 10(b) are basically consistent. As expected, the cell size obtained after "3D watershed split" is slightly larger than the ones obtained by "Local Thickness". The difference of the two methods could be reflected by the comparison of average cell diameters for all of these distributions for all the samples. This is gathered in Fig. 11. It can be seen that the cell size obtained after "3D watershed split" is typically about 30% larger than the one obtained by "Local Thickness". Even if the splitting is not absolutely perfect, the result after using "3D watershed split" is considered more reliable. This is because in the other method, some regions located close to the boundaries of cells are artificially measured to contribute to smaller sizes in the distribution. This systematic error increases with the decrease of sphericity. However, "Local Thickness" is a good and straightforward way to estimate the cell size distribution of aluminium foams, especially when the cells are connected to some extent.

The equivalent diameter is plotted as a function of the sphericity for each splitted cell in eight different representative foam samples in Fig. 12. In the case of MF foams, there are usually large cells whose size is much bigger than the average cell size, as shown by the red circles in Fig. 12(a), (b) and (c). Fig. 12(i) displays the internal large cells in the foam of Fig. 12(b), which could also be seen in Fig. 8(b). It indicates that cells merging occurs frequently during MF preparation process, which is due to the difficulty of controlling the distribution and decomposition of $TiH_2$. In the case of dynamic GI foams, it is rather clear that the distribution of cell sizes is wide. This is mainly because the cell sizes are usually not uniform in one cycle of high-speed horizontal vibration [40]. Moreover, the disturbance of the liquid melt caused by the vibration may also affect the uniformity of the bubble size. It can be observed from Fig. 12(g) and (h) that the aluminium foams prepared by static GI method have a better cell size uniformity and a more concentrated sphericity distribution, especially for the foam of Fig. 12(h). Most cell sizes of the foam in Fig. 12(h) are centered in the range of 4–5 mm, which is almost also the smallest cell size that static GI method can achieve. It can also be concluded from Fig. 12 that the sphericity distribution of GI foams is better than that of MF foams. One of the reasons is that the shape of the bubbles could possibly be adjusted a little during the floating process of the GI method. Another reason is that the merging of small pores and large pores affects the sphericity of the final cell in MF method.

Fig. 13 shows the numerical average of the cell equivalent diameter (calculated from the splitting method) of aluminium foams prepared by different methods plotted as a function of the porosity in each sample. It can be seen that average diameter of aluminium foams increases sharply when the value of porosity increases. The aluminium foam with the smallest cell size was obtained by MF method. Aluminium foams prepared by static GI method are usually larger in cell size compared to the ones prepared by other methods. Dynamic GI method could significantly reduce the cell size compared to the static method. The aluminium foam with smaller cell size and higher porosity can be obtained by dynamic GI method combined with smaller particles. When the

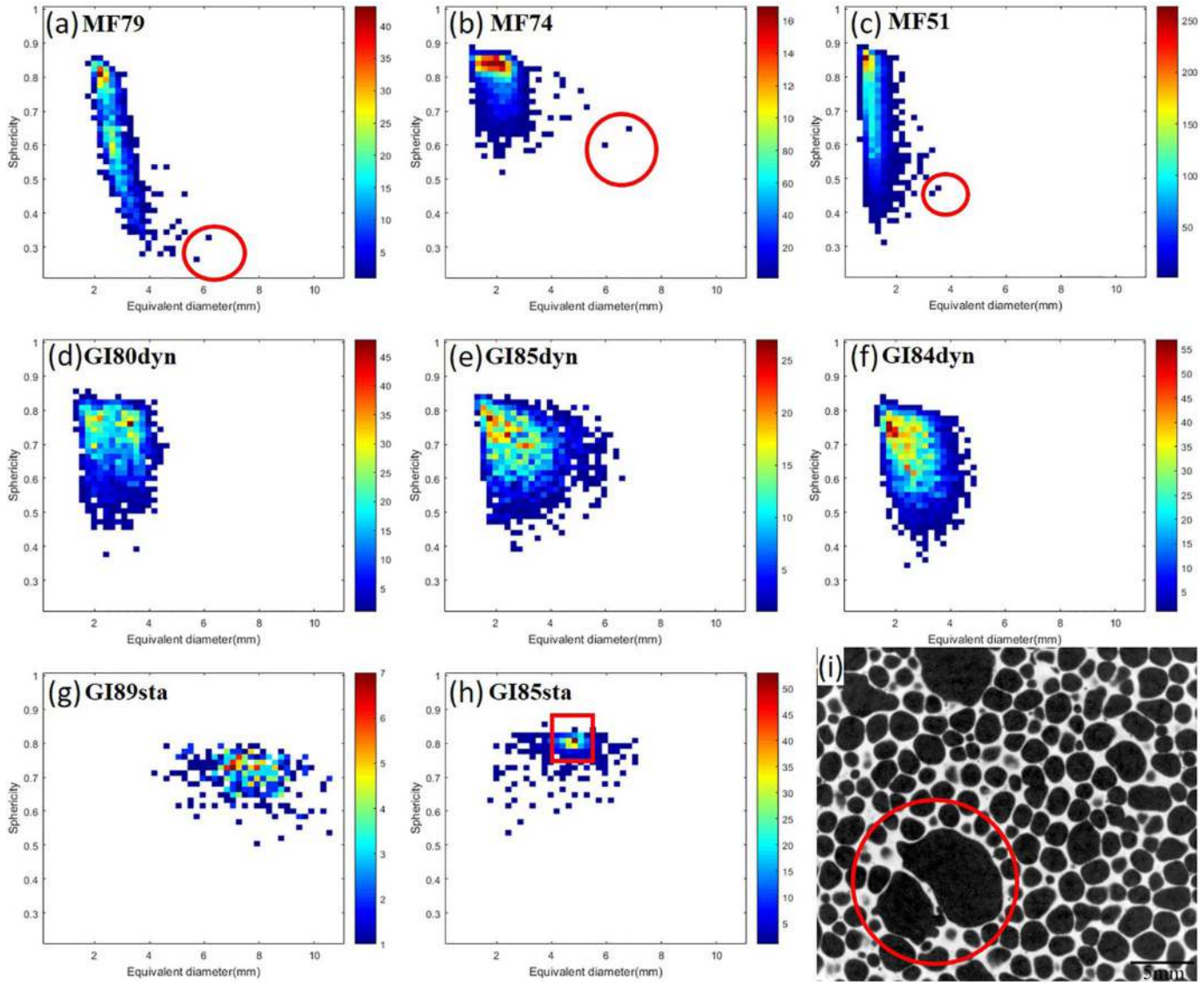


**Fig. 12.** Distributions of equivalent diameter and sphericity of cells in different aluminium foams, (a) MF79, (b) MF74, (c) MF51, (d) GI80dyn, (e) GI85dyn, (f) GI84dyn (g) GI89sta and (h) GI85sta. (i) the internal large cells in the foam of Fig. 12(b).

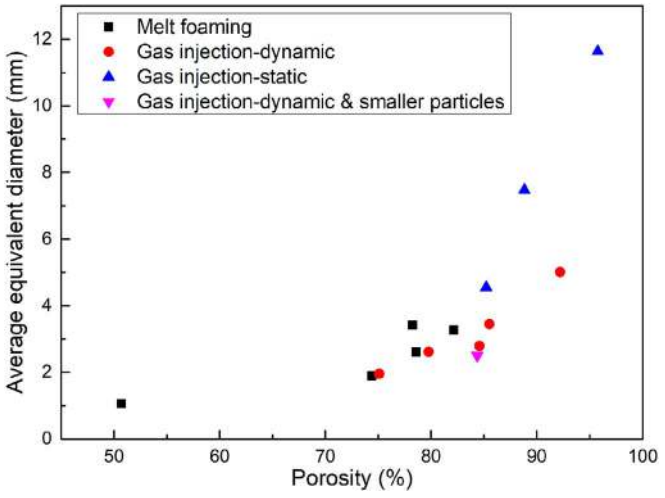


**Fig. 13.** Variation of the average cell equivalent diameter with overall porosity of aluminium foams prepared by different methods.

average cell diameters are almost the same, the porosity of dynamic GI samples is usually higher than that of MF samples under their respective matrix. So GI method is more suitable to prepare aluminium foams with high porosity compared to MF method. Contrarily, aluminium foams with high density could be obtained by MF method through reducing the amount of $TiH_2$.

### *3.5. Solid Material Thickness Difference of Aluminium Foams Prepared by Different Methods*

The "Local Thickness" plugin was also used to determine the solid material thicknesses of different foams. As shown in Fig. 14, when coloured according to their local thickness by the plugin, the typical size of the solid material can be measured. Fig. 15 illustrates the distributions of solid material thickness in different aluminium foams. In the case of MF foams, the solid material thickness distributions show a trend of the normal distribution, most of the solid material thicknesses distribute in the middle region. In the case of GI foams, the thickness distribution is more of a log-normal type, and most of the solid material thicknesses are in the thinner solid material region. This feature is even more pronounced in static GI foams. The wall thickness of Plateau border is larger than the normal wall thickness between two cells

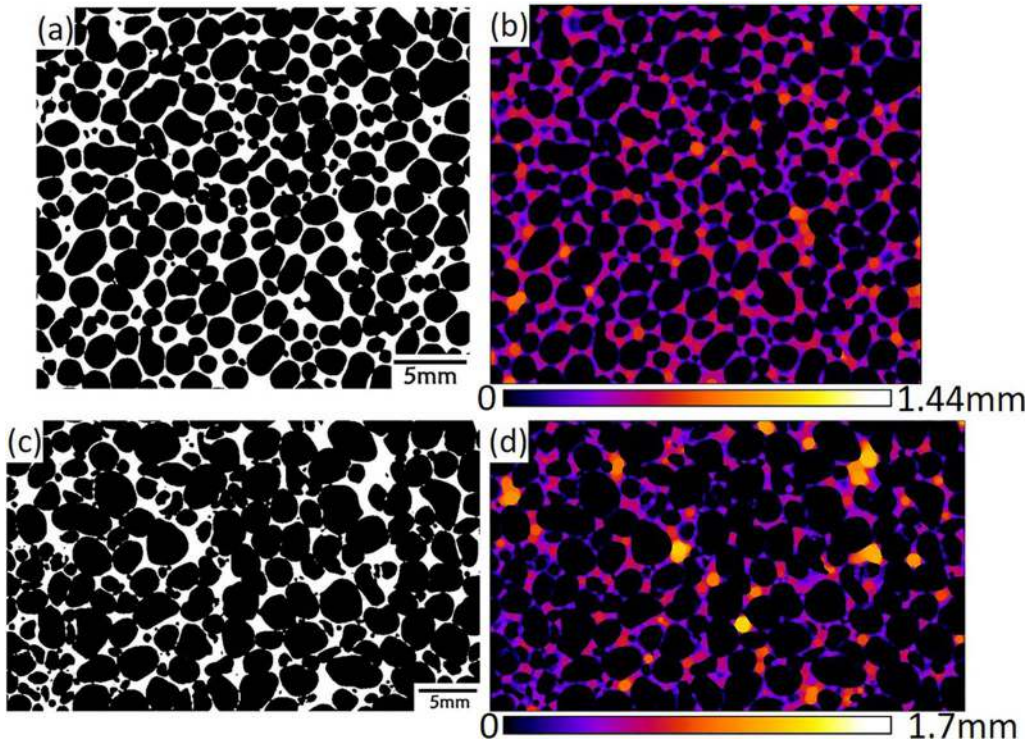


**Fig. 14.** (a) Binarized image and (b) the image after calculating with "Local Thickness" for solid material thickness of the MF74 (the calculated average solid material thickness $\bar{t}$ is 0.378 mm, and the standard deviation $s$ is 0.154 mm), (c) binarized image and (d) the image after calculating with "Local Thickness" for solid material thickness of the GI80dyn ($\bar{t}$ is 0.459 mm, and $s$ is 0.256 mm).

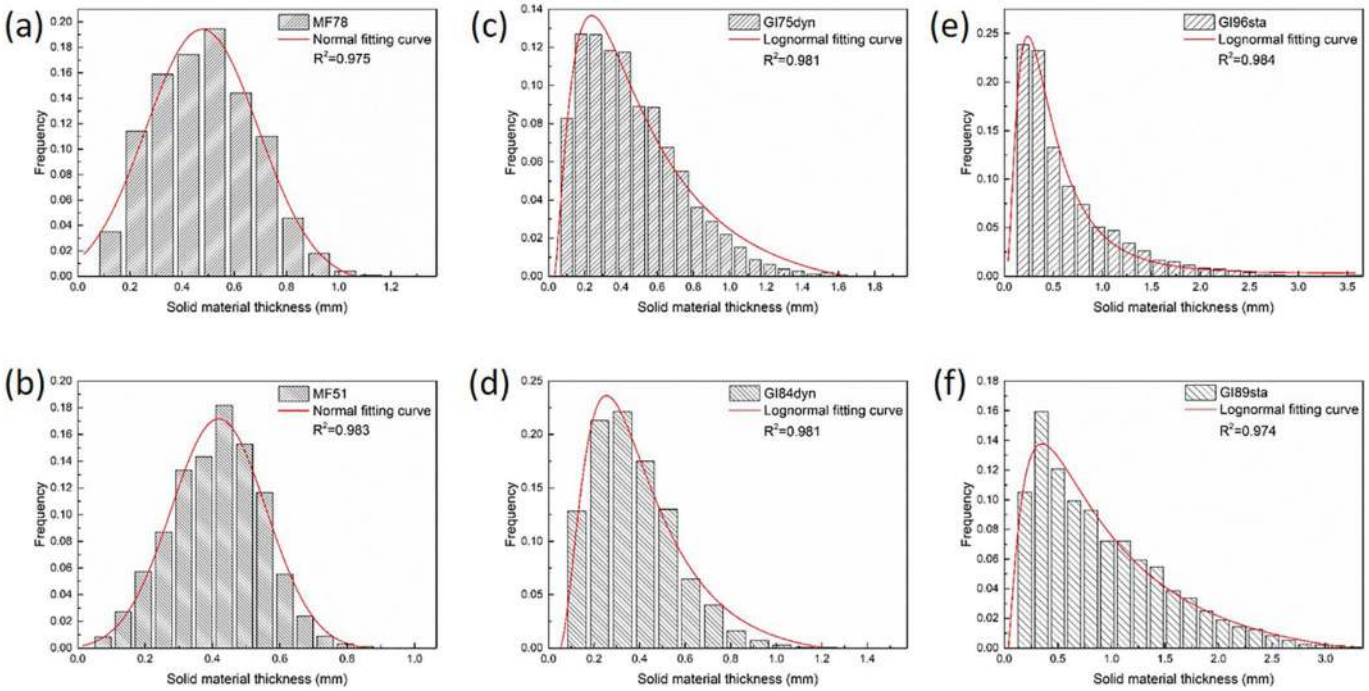


**Fig. 15.** Distributions of the solid material thickness in different aluminium foams (a) MF78, (b) MF51, (c) GI75dyn, (d) GI84dyn, (e) GI96sta and (f) GI89sta.

[37,38], so the larger thickness in Fig. 15 is usually attributed by Plateau borders. According to the different distribution characteristics of the solid material thickness in different aluminium foams, the thickness difference between normal cell wall and Plateau border in MF foams is smaller than the one in GI foams, which could also be reflected by the cell wall morphology in Fig. 4. Therefore, the amount of liquid drainage in bubbles walls during the preparation process of GI method is more important than that of MF method under their respective matrix. The bubbles could remain closed in the case of serious drainage for GI foams, which is related to the oxide film on the surface of bubbles during the solidification process. It could also be seen from Fig. 15 that the proportion of Plateau border is correspondingly less because of the larger cells in static GI foams.

Then the average solid material thickness of different aluminium

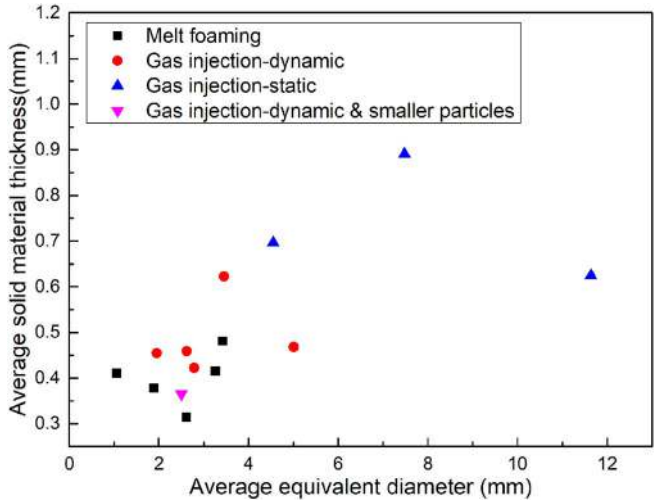


**Fig. 16.** Variation of the average solid material thickness with average cell equivalent diameter of aluminium foams prepared by different methods.

foams could also be obtained, as Fig. 16 shows. It can be seen that the average solid material thickness of static GI foams is quite higher than the ones prepared by other methods, which is also related to the larger cell size of static GI foams and to the fact that the wall thickness scales homothetically with the cell size. When the average cell diameters are almost the same, the average solid material thickness of the MF foam is smaller than that of the GI foam under their respective matrix. In the case of GI foams, the foam with small cell size and thin solid material can be obtained when the dynamic method and smaller ceramic particles are used.

## 4. Conclusions

1) The closed porosity of the aluminium foam prepared by MF method is much lower than the one prepared by GI method at a similar overall porosity, which is related to the bubble formation processes of different aluminium foams. In the case of the MF method, the closed porosity can be improved by increasing the relative density.
2) There are more micropores in cell walls of aluminium foams prepared by MF method than that in aluminium foams prepared by GI method, especially for the MF foam with low porosity. Micropores in static GI foams were less than the ones in dynamic GI foams.
3) The cell size obtained after “3D watershed split” is, as expected, larger than the one obtained by “Local Thickness”. Dynamic GI foams have a smaller cell size and wider cell size distribution compared to static GI foams. In addition, there are usually big holes inside MF foams. GI method is more suitable to prepare aluminium foams with high porosity compared to MF method under a similar cell size condition.
4) The thickness difference between normal cell wall and Plateau border is greater in GI foams compared to MF foams, in particular for the static GI method.

## Acknowledgements

This work is supported by the International Cooperation Project of Science and Technology Ministry of China (Grant no. 2013DFR50330). The authors would like to thank the Tsinghua Scholarship for Overseas Graduate Studies.

## References

[1] J. Banhart, Light-metal foams-history of innovation and technological challenges, Adv. Eng. Mater. 15 (2013) 82–111.
[2] J. Banhart, Metal foams: production and stability, Adv. Eng. Mater. 8 (2006) 781–794.
[3] T. Miyoshi, M. Itoh, S. Akiyama, A. Kitahara, ALPORAS aluminium foam: production process, properties, and applications, Adv. Eng. Mater. 2 (2000) 179–183.
[4] I. Jin, L.D. Kenny, H. Sang, Method of producing lightweight foamed metal, USA Patent 4973358, 1990.
[5] H. Sang, L.D. Kenny, I. Jin, Process for producing shaped slabs of particle stabilized foamed metal, USA Patent 5334236, 1994.
[6] W. Ruch, B. Kirkevag, A process of manufacturing particle reinforced metal foam and product thereof, European Patent 0483184B1, 1990.
[7] F. Dobesberger, H. Flankl, D. Leitlmeier, A. Birgmann, Device and process for producing metal foam, USA Patent 7195662B2, 2007.
[8] D. Leitlmeier, H.P. Degischer, H.J. Flankl, Development of a foaming process for particulate reinforced aluminium melts, Adv. Eng. Mater. 4 (2002) 735–740.
[9] Y. Sugimura, J. Meyer, M.Y. He, H. Bart-Smith, J. Grenstedt, A.G. Evans, On the mechanical performance of closed cell Al alloy foams, Acta Mater. 45 (1997) 5245–5259.
[10] J. Banhart, Manufacture, characterisation and application of cellular metals and metal foams, Prog. Mater. Sci. 46 (2001) 559–632.
[11] Y. Li, Comparison of aluminium foams produced by melt foaming and gas injection processes, Spec. Cast. Nonferrous Alloys. 31 (2011) 1097–1099.
[12] A.E. Simone, L.J. Gibson, Aluminium foams produced by liquid-state processes, Acta Metall. 46 (1997) 3109–3123.
[13] A. Elmoutaouakkil, L. Salvo, E. Maire, G. Peix, 2D and 3D characterization of metal foams using X-ray tomography, Adv. Eng. Mater. 4 (2002) 803–807.
[14] H. Zhang, X. Chen, X. Fan, Y. Li, Compressive properties of aluminium foams by gas injection method, China Foundry 9 (2012) 215–220.
[15] T. Shi, X. Chen, Y. Cheng, Y. Li, Foaming process and properties of 6063 aluminium foams by melt foaming method, Mater. Trans. 58 (2017) 243–248.
[16] Y. Zou, D. He, J. Jiang, New type of spherical pore Al alloy foam with low porosity and high strength, Sci. China Ser. B Chem. 47 (2004) 407–413.
[17] J. Yuan, Y. Li, Effects of cell wall property on compressive performance of aluminium foams, Trans. Nonferrous Metals Soc. China 25 (2015) 1619–1625.
[18] W. Gan, S. He, D. He, Y. Zhang, L. Wang, D. Tong, Preparation and compressive property of foam aluminium with high porosity and small pore diameter, Mater. Mech. Eng. 34 (2010) 45–48.
[19] Y. Cheng, Y. Li, X. Chen, T. Shi, Z. Liu, N. Wang, Fabrication of aluminium foams with small pore size by melt foaming method, Metall. Mater. Trans. B Process Metall. Mater. Process. Sci. 48 (2017) 754–762.
[20] N. Babcsan, S. Beke, P. Makk, P. Soki, G. Szamel, H.P. Degischer, R. Mokso, ALUHAB - the superior aluminium foam, 13th International Conference on Aluminium Alloys (ICAA13), 2012, pp. 1005–1010.
[21] N. Babcsan, S. Beke, P. Makk, G. Szamel, C. Kadar, Pilot production and properties of ALUHAB aluminium foams, Procedia Mater. Sci. 4 (2014) 127–132.
[22] F. García-Moreno, B. Siegel, K. Heim, A.J. Meagher, J. Banhart, Sub-mm sized bubbles injected into metallic melts, Colloids Surf. A Physicochem. Eng. Asp. 473 (2015) 60–67.
[23] N. Wang, X. Chen, Y. Li, Z. Liu, Z. Zhao, Y. Cheng, Y. Liu, H. Zhang, The cell size reduction of aluminium foam with dynamic gas injection based on the improved foamable melt, Colloids Surf. A Physicochem. Eng. Asp. 527 (2017) 123–131.
[24] N. Babcsan, S. Beke, P. Makk, Method of producing a metal foam by oscillations and thus obtained metal foam product, World Patent WO 2010/064059 A2, 2010.
[25] W. Jang, W. Hsieh, C. Miao, Y. Yen, Microstructure and mechanical properties of ALPORAS closed-cell aluminium foam, Mater. Charact. 107 (2015) 228–238.
[26] E. Maire, X-ray tomography applied to the characterization of highly porous materials, Annu. Rev. Mater. Res. 42 (2012) 163–178.
[27] E. Maire, J. Adrien, C. Petit, Structural characterization of solid foams, C. R. Phys. 15 (2014) 674–682.
[28] C. Petit, S. Meille, E. Maire, Cellular solids studied by x-ray tomography and finite element modeling - a review, J. Mater. Res. 28 (2013) 2191–2201.
[29] L. Salvo, P. Belestin, E. Maire, M. Jacquesson, C. Vecchionacci, E. Boller, M. Bornert, P. Doumalin, Structure and mechanical properties of AFS sandwiches studied by in-situ compression tests in X-ray microtomography, Adv. Eng. Mater. 6 (2004) 411–415.
[30] L.J. Gibson, M.F. Ashby, Cellular Solids: Structure and Properties, Cambridge University Press, Cambridge New York, 1997.
[31] R.E. Raj, V. Parameswaran, B.S.S. Daniel, Comparison of quasi-static and dynamic compression behavior of closed-cell aluminium foam, Mater. Sci. Eng. A Struc. Mater. Proper. Micro. Process. 526 (2009) 11–15.
[32] T. Ohgaki, H. Toda, M. Kobayashi, K. Uesugi, M. Niinomi, T. Akahori, T. Kobayash, K. Makii, Y. Aruga, In situ observations of compressive behaviour of aluminium foams by local tomography using high-resolution X-rays, Philos. Mag. 86 (2006) 4417–4438.
[33] M. Mukherjee, F. García-Moreno, C. Jiménez, A. Rack, J. Banhart, Microporosity in aluminium foams, Acta Mater. 131 (2017) 156–168.
[34] D.Q. Wang, Relation of cell uniformity and mechanical property of a close cell aluminium foam, Adv. Eng. Mater. 15 (2013) 175–179.
[35] X. Yang, W. Wang, L. Yan, Q. Zhang, T.J. Lu, Effect of pore morphology on cross-property link for close-celled metallic foams, J. Phys. D. Appl. Phys. 49 (2016) 505301.
[36] J. Kadkhodapour, S. Raeisi, Micro–macro investigation of deformation and failure in closed-cell aluminium foams, Comput. Mater. Sci. 83 (2014) 137–148.
[37] D.Q. Wang, X. Meng, W. Xue, Z. Shi, Effect of processing parameters on cell structure of an aluminium foam, Mater. Sci. Eng. A 420 (2006) 235–239.
[38] D.Q. Wang, W. Xue, X. Meng, Z. Shi, Cell structure and compressive behavior of an aluminium foam, J. Mater. Sci. 40 (2005) 3475–3480.
[39] J. Yuan, Y. Li, N. Wang, Y. Cheng, X. Chen, Effect of orifice diameter on bubble

generation process in melt gas injection to prepare aluminium foams, Metall. Mater. Trans. B Process Metall. Mater. Process. Sci. 47 (2016) 1649–1660.
[40] N. Wang, X. Chen, J. Yuan, G. Wang, Y. Li, H. Zhang, Y. Liu, Bubble formation at a submerged orifice in high-speed horizontal oscillation, Metall. Mater. Trans. B Process Metall. Mater. Process. Sci. 47 (2016) 3362–3374.
[41] J.Y. Buffiere, E. Maire, J. Adrien, J.P. Masse, E. Boller, In situ experiments with X ray tomography: an attractive tool for experimental mechanics, Exp. Mech. 50 (2010) 289–305.
[42] C. Petit, E. Maire, S. Meille, J. Adrien, Two-scale study of the fracture of an aluminium foam by X-ray tomography and finite element modeling, Mater. Des. 120 (2017) 117–127.
[43] E. Maire, A. Elmoutaouakkil, A. Fazekas, L. Salvo, In situ X-ray tomography measurements of deformation in cellular solids, MRS Bull. 28 (2003) 284–289.
[44] E. Maire, P. Colombo, J. Adrien, L. Babout, L. Biasetto, Characterization of the morphology of cellular ceramics by 3D image processing of X-ray tomography, J. Eur. Ceram. Soc. 27 (2007) 1973–1981.
[45] C. Indhumathi, Y.Y. Cai, Y.Q. Guan, M. Opas, An automatic segmentation algorithm for 3D cell cluster splitting using volumetric confocal images, J. Microsc. 243 (2011) 60–76.
[46] Y. Zhou, Y. Li, J. Yuan, The stability of aluminium foams at accumulation and condensation stages in gas injection foaming process, Colloids Surf. A Physicochem. Eng. Asp. 482 (2015) 468–476.
[47] K. Heim, G.S. Vinod-Kumar, F. García-Moreno, A. Rack, J. Banhart, Stabilisation of aluminium foams and films by the joint action of dispersed particles and oxide films, Acta Mater. 99 (2015) 313–324.
[48] D. Li, T. Sun, G. Yao, X. Zhang, J. Li, Preparation of foam aluminium with small pores by melt-based route of $ZrH_2$, Chin. J. Nonferrous Met. 01 (2010) 143–148.